Available online at www.sciencedirect.com

SciVerse ScienceDirect

Advances in Space Research 51 (2013) 76–86

ADVANCES IN SPACE RESEARCH (a COSPAR publication)

www.elsevier.com/locate/asr

The spatial distributions of the sources of UV solar Explosive Events at different velocities

J.E. Mendoza-Torres *

Instituto Nacional de Astrofísica, Optica y Electrónica, Calle Luis Enrique Erro No. 1, C.P. 72840, Sta. María Tonantzintla, Puebla, Mexico

Received 22 November 2011; received in revised form 21 July 2012; accepted 30 August 2012
Available online 11 September 2012

Abstract

We analyze five solar Explosive Events observed in the Si IV emission line at 139.37 nm during SUMER/SoHO raster scans near disk center. The Doppler velocities from $-45\ km\ s^{-1}$ to $+45\ km\ s^{-1}$ were sorted into eleven symmetrically organized velocity bins, five equally-sized bins on each side and one bin for the line at rest. The radiance values along the NS oriented slit around the maximum of each EE are used to build one-dimensional distributions. We study these distributions and their development in space and time for different velocity bins to unveil the 3D-structure and evolution of Explosive Events. The spatial radiance distributions for the EE maximum and around it were made. For some Explosive Events the dispersion direction is not oriented orthogonally to the slit direction; consequently, the blueshifted emission is in a linear way offset from the redshifted emission by several pixels. The largest offset ($\sim 5''$) is observed between distributions whose velocities differ by $\sim 36\ km\ s^{-1}$. The linear relation agrees with an scenario of flows inside magnetic arcs.

Keywords: Sun; Explosive Events; UV radiance

1. Introduction

Explosive Events (EE) have been observed at different lines in the far UV (FUV) wavelength range (Brueckner and Bartoe, 1983; Dere, 1994) and are characterized by their Doppler flow at high resolution spectra of emission lines released at TR temperatures. They have typical sizes of few arcseconds, lifetimes of few minutes and velocities of up to $\sim 250\ km\ s^{-1}$ (Pérez et al., 1999; Teriaca et al., 2002 and Ning et al., 2004).

Some photospheric and chromospheric transient phenomena that are thought to be the result of release of magnetic energy have been found to be related to coronal phenomena. The EEs are probably the smallest transient events thought to be related to magnetic reconnection (Innes et al., 1997). They are spatially small but many of them are simultaneously taking place all over the Sun (Brueckner and Bartoe, 1983). For this reason they could give a non-negligible input for coronal heating.

To unveil the nature of EE one has to present a convincing model that can reproduce the stationary character, the high Doppler flow and other characteristics of features near the spatial resolution of modern spectrometers. This is important to have an insight on how EE can affect different layers of the solar atmosphere.

In this work the radiance spatial distributions at several Doppler velocities are built to see details of the plasma flows at EE. The spatial distributions with velocities up to $\sim 40\ km\ s^{-1}$, which could be close to the origin of the flows at small spatial scales, are analyzed.

1.1. Line profiles

EE are characterized by their Doppler flow that have been only seen in emission lines released at TR temperatures. During EEs the line profiles are frequently asymmetric (Teriaca et al., 2002) indicating differences between the

* Tel.: +52 222 2663100; fax: +52 222 2472231.
E-mail address: mend@inaoep.mx.

0273-1177/$36.00 © 2012 COSPAR. Published by Elsevier Ltd. All rights reserved.
http://dx.doi.org/10.1016/j.asr.2012.08.015

emitting plasma source flow responsible for red and blue brightenings (Ning et al., 2004). Some EE are well fitted by two or three Gaussians allowing to consider the presence of red or/and blue flows (Mendoza-Torres et al., 2009). However, in many other cases the profiles are neither Gaussian nor the sum of them (Brueckner and Bartoe, 1983). When fitting a Gaussian the amplitude of several velocity bins is used to determine the highest radiance, location and size of a source as if all the emission recorded at these velocity bins would be cospatially produced. Then, small differences between the sources of plasma at different velocities could be missed.

An alternative way to study plasma flows may be based on the analysis of the radiance at each spectral channel. Rompolt (1975) analyzed data of different solar features as filaments and loops and found that the orientation and shape of the spectral features, along the slit, agree with emission expected for some given geometries and view angles. To obtain the diagram of spectral features only one wavelength is considered, i.e., broadening is neglected.

The identification of the behavior of the spectral features could give an insight into the geometry of the sources of EEs and into the behavior of the flows produced at them.

For the below analysis we consider an EE source as a region where the next two characteristics are observed: (a) The temporal enhancement of red and/or blue wings and (b) The increase and decrease of the line radiance coincident with the wing enhancement.

SUMER observations of the Si IV line have shown to be suitable for the study of EE (Ning et al., 2004). In this work, we build the spatial distributions for plasma at different velocity based on the radiance at different bins of the Si IV 139.37 nm emission line. This method is applied here for the first time to the study of EE.

2. Observations

The data set was obtained on June 20, 1996 employing a $1'' \times 120''$ slit. For the SoHO distance at that epoch 1 pixel equals 715 km. The readout window was centered at the Si IV line at 139.37 nm with a spectral resolution of 0.45 nm and a total width of 50 spectral pixels.

In order to study the spatial distribution of EE we selected the raster mode with high cadence (six EW positions of 5 s integration each). This mode consists of cycles where two runs are made in a cycle. In the first run the slit is sequentially directed to the EW odd positions 1, 3 and 5 of Fig. 2 that correspond to $-1.5''$, $0''$ and $1.5''$ respect an imaginary NS straight line across the disk center (L_{NSC}), where negative values are for positions at the East side and positive to the West side of L_{NSC}. In the second run the slit is directed to the three even positions 2, 4 and 6 that correspond to $-0.75''$, $0.75''$ and $2.25''$. Therefore, a $\sim 5'' \times 120''$ EW-NS field is covered. At each EW position 120 spectra are obtained, each for a NS pixel along the slit with a time integration of 5 s.

3. Selection of the EE

An IDL routine identified the positions and times of maximum values over the entire time interval observed over the whole scanned area. Once the time and location of the first maximum was identified a new search of the maximum value was done excluding a 3 pixels × 3 pixels area around the first maximum. This routine gave us an initial set of potential EE.

It is more easy to identify wing variations at intense spectral lines rather than at weak ones. For this reason we selected the EEs with higher radiance of our sample. It means, the maximum line radiance of the events was also considered to select our sample. The cases where the maximum radiance was at least 5σ higher than radiance observed 1.5 min before and also was $5\,\sigma$ higher than 1.5 min after it were considered as EE.

From the resulting sample we selected only those cases where the maximum took place at an EW position from 2 to 5. It means EE were selected such that their maximum was not at the extremes of the field of view. The selection included only EEs that could be observed at least two time intervals before and two time intervals after the maximum.

After the identification of the strongest EE the brightness maxima at velocity bins close to the central one were measured. Four velocity bins on the blue side of the rest wavelength channel and four on the red side were analyzed for each selected EE. In some particular cases six velocity bins on each side were analyzed.

4. Arrays of spectra

The line profiles around the brightness peak were plotted in a 6 EW × 9 NS array (mosaic of plot panels), as in Fig. 2. The columns correspond to the EW positions $-1.50''$, $-0.75''$, $0.00''$, $0.75''$, $1.50''$ and $2.25''$. This means that the third column was pointing towards the L_{NSC}.

The bottom panels are for the slit NS position 40 or 10″S respect an imaginary EW straight line that crosses the solar disk center (L_{EWC}) and the panels at the top are for NS slit position 48 or 2″S. Further we use positive values for locations above the L_{EWC} and negative for locations below it. This means that negative values are for locations below the disk center.

For Fig. 2 the line profiles at columns 1, 3 and 5 correspond to observed values. The slit is directed to that locations at the times given in the second panel from top to bottom (at the corresponding columns).

The line profiles for the even positions 2, 4 and 6 are averaged from values taken at the previous and the further runs at each given EW location. It may be seen that the line profile and amplitude vary from one place to other.

5. North–South spatial distributions

For each EE the maxima at different velocity bins of the Si IV spectral line at each EE were measured. The bins are

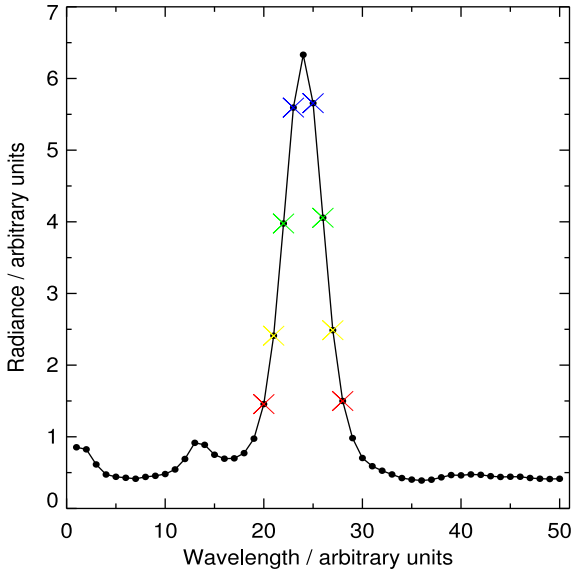

Fig. 1. Spectral line averaged over regions of weak radiance. The more intense spectral feature corresponds to the 139.37 nm Si IV line. At shorter wavelengths the 139.33 nm Ni II and the 139.28 Fe II lines are present. The crosses are at the spectral pixels at which the amplitudes were used to build the one-dimensional distributions of EE sources. The blue crosses correspond to the velocity bins closest to the central one on both sides of the line (red and blue) with a Doppler velocity of 9 km s^{-1}. The colors used here stand for the respective distributions in the following figures, blue lines correspond to these velocities with both red and blue Doppler shifts. The green lines are for the 18 km s^{-1} Doppler shifted sources, yellow for 27 km s^{-1} and red for 36 km s^{-1}. (For interpretation of the references to colour in this figure legend, the reader is referred to the web version of this article.)

indicated in Fig. 1. NS distributions for the center velocity bin were made for times before and after the maximum (Fig. 3). Also, the average of the amplitudes of two consecutive NS pixels (moving average) for a given bin was computed. These values were also plotted, as below described. The NS distributions were made for 9 bins, four bins on each line side and the central one.

Plots with 5 curves were made, the central wavelength, 4 distributions for velocity bins on the red side and 4 distributions for bins on the blue one. In Fig. 4 examples of NS distributions for various spectral pixels (further also referred to as velocity bins) are shown. At this figure and at subsequent figures the times are indicated in each panel. There is a difference of ~9 km s^{-1} between the velocities of two consecutive velocity bins. Further, we will use the term blue, central or red distribution to refer respectively to blue bin, central bin or red bin distribution. In some cases to refer to a particular velocity bin we will use the velocity that corresponds to that bin.

In Fig. 4 and in similar figures the black lines correspond to the central, the blue lines are for 9 km s^{-1}, green for 18 km s^{-1}, yellow for 27 km s^{-1} and red for 36 km s^{-1} distributions. Positive values in the NS scale are for locations at the South and negative at the North of L_{EWC}. The distributions at Fig. 4 are smoothed due to the averaging of two consecutive NS values while the distributions shown at Fig. 3 are not smoothed.

NS distributions, as those of each panel of Fig. 4, from about 5 min before and after each EE maximum, for the six EW positions of the raster observations were also made. Further, to refer to a given EW position we will simply write EW followed by the number of the corresponding EW position. For example, instead o EW position 5 we will simply write EW 5.

For some times and locations the radiance distributions at an additional spectral bin at each line side were analyzed, giving in those cases a total of eleven bins.

6. Results

We have made plots for the strongest five EE of the sample, here the NS distributions at and around the location of the maximum of each of them are analyzed. We consider as the EE source a region where the increase and decrease of the radiance were observed.

In most of the cases the maxima amplitudes of the different velocity distributions differ to each other. The maximum decreases as going from the central distribution to the 36 km s^{-1} one and their maxima are roughly at the same location. However, at some locations the maxima of the different velocity distributions are offset with respect each other. Also, at some other locations the amplitudes of different velocity distributions are similar to each other. Further, we describe each of the observed EE.

6.1. EEI, maximum at 14:14:35 UT

The maximum of this EE took place at 14:14:35 UT at EW position 5 (which is 1.5″ to the West of L_{EWC}) and NS −6″, which in a plot as that of Fig. 2 will correspond to the row number (slit pixel) number 55. The amplitude remains at high amplitudes for about 2 min which indicates a slower radiance decay than the increase for this EE (left panel of Fig. 3).

In this EE offsets of the radiance maxima are seen at some given locations near the EE maximum, including the time and location of the maximum (left panel of Fig. 4).

The extensions and locations of the maxima of the radiance distributions of different spectral pixels differ to each other. Also, time variations are seen. The radiance at the maximum and at locations around it is higher at red than at blue distributions.

At the EE shown at the left panel of Fig. 4 which corresponds to the time and location of the EE maximum, the 36 km s^{-1} red maximum is offset to the North about 2″(~1.5 Mm) respect the maximum of the central distribution. Similar offsets are observed at other EE. At the time and location of the maximum of this EE no offsets are observed for the blue distributions. However, 1.3 min after the EE maximum, at about 1.5″ to its East, the 36 km s^{-1} blue distribution is offset ~2″ to the South respect the central one.

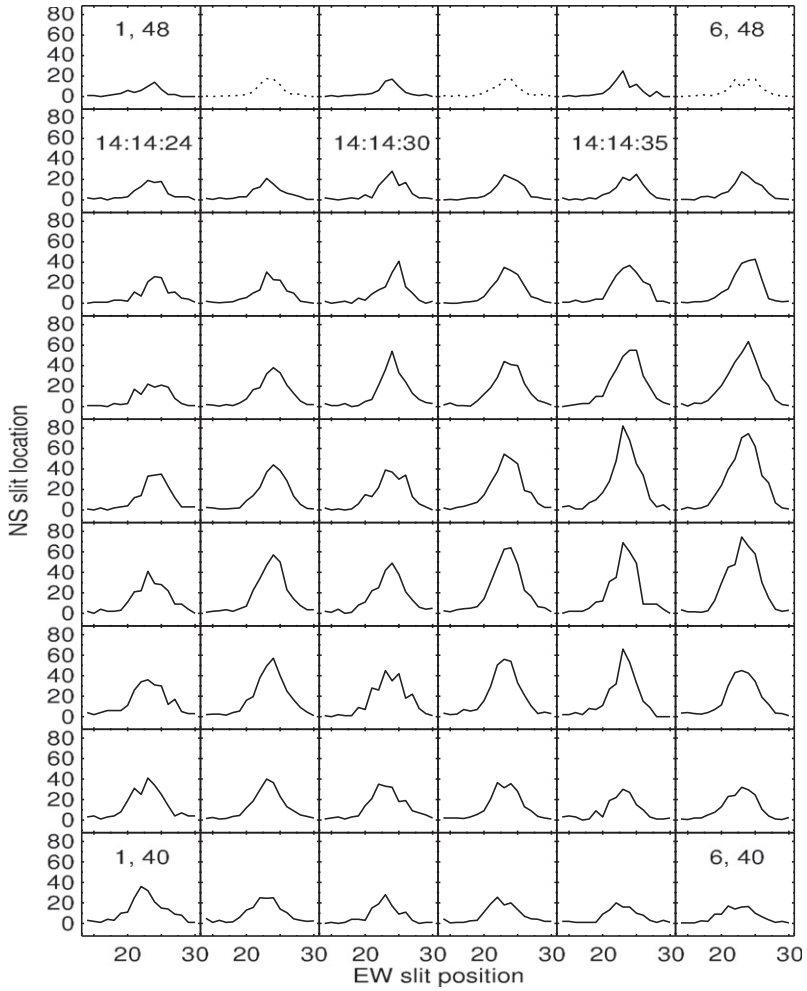

Fig. 2. Array of spectra as observed at positions around one of the Explosive Events analyzed here (later referred to as EEI). Columns correspond to EW raster positions and rows to pixels along the slit. At each panel the inner x-axis correspond to wavelength in arbitrary units and the inner y-axis to radiance in arbitrary units. The maximum took place at EW 5, NS 44 at 14:14:35 UT. The column with dotted spectral lines at the top corresponds to the line profiles obtained by averaging the profiles before and after (see text) while the columns where the spectral line at the top is solid correspond to observed profiles.

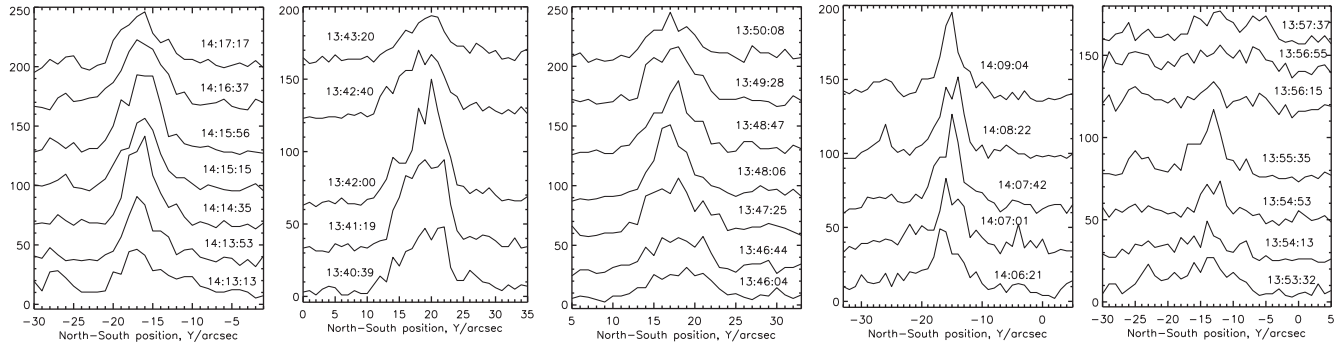

Fig. 3. NS radiance distributions for the central spectral pixel for the five observed EE. The time grows from lower to upper curves, the time is given in each curve. In the x-scale of each panel the NS position respect the L_{NSC} line is given, positive are for values above and negative below this line. In the y-scale the radiance is given in arbitrary units. The distributions for different times are vertically offset by about 30–50 counts in order to allow a better view of the features of the distributions.

Offsets between red and blue maxima are seen at locations from $\sim 0.8''$ to $\sim 1.5''$ at both, West and East sides of the EE maximum (Fig. 5). The offset between blue and red distributions is seen to increase with velocity. In this

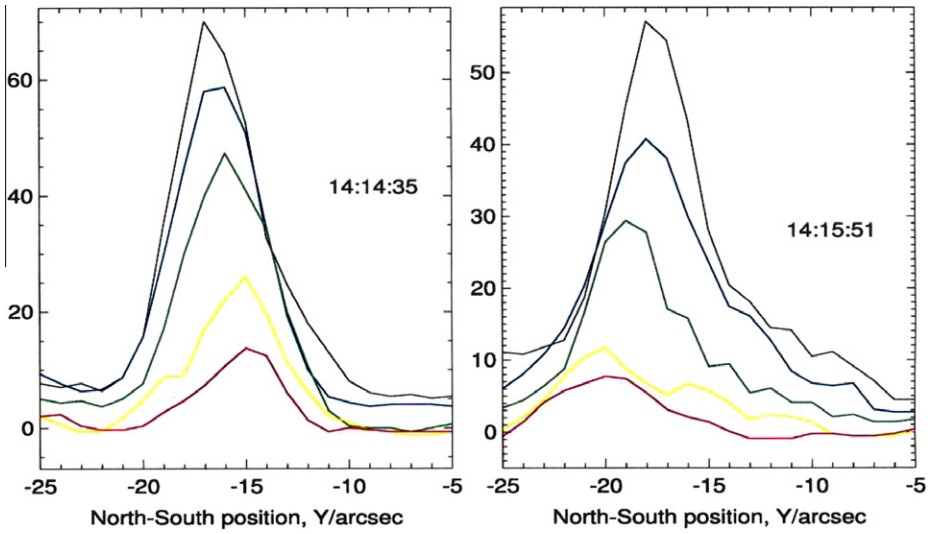

Fig. 4. NS red distributions at the time and location of the EEI maximum (left) and blue distributions observed 1 min 16 s after it, 1.5″ at the East of the maximum (right). In both cases offsets between the maxima of the different velocity distributions are seen. According to Rompolt (1974), this effect is similar to the spectral tilted line expected by a cylinder or by a sphere. At the left panel distributions the higher velocity maxima are at the North respect the lower velocity ones and at right panel distributions the offset of the higher velocity maxima is to the South respect the lower velocity ones.

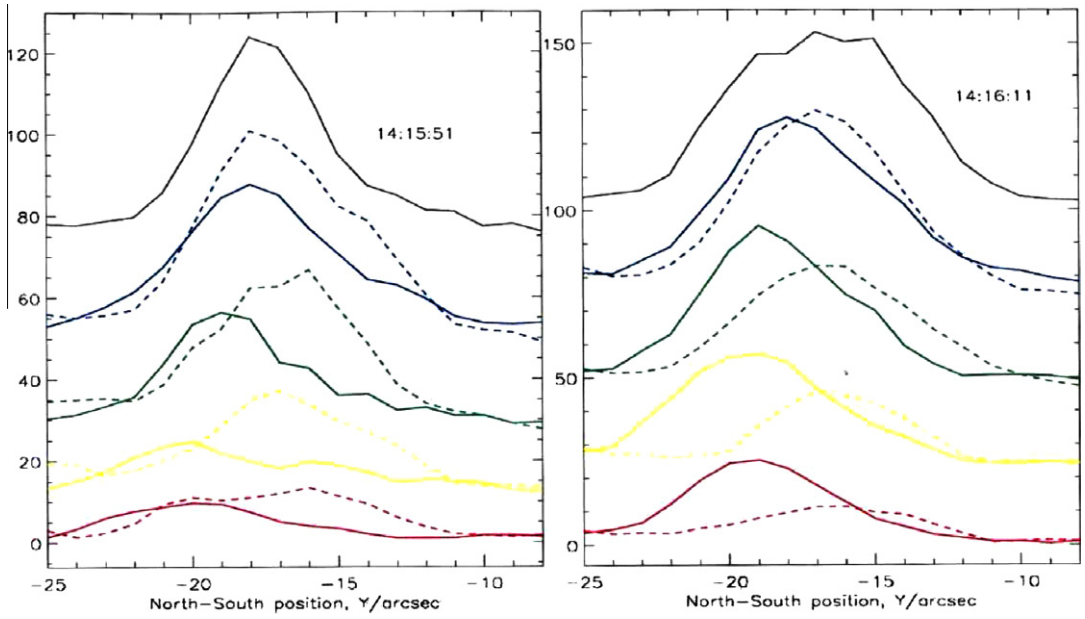

Fig. 5. NS blue (solid lines) and red distributions (dashed lines) observed 1 min 16 s after the EEI maximum, at ~1.5″ on its East side (left). Blue and red distributions observed ~0.8″ on the East of the maximum, 1 min 35 sec after it (right). It may be seen that in both cases the blue distributions are at the South respect the red distributions. The offset between the red and blue maxima of the highest velocity distributions is larger than for lower velocity maxima. The offset increases with velocity.

particular case, the offset was observed for more than 1 min. The locations of the maximum as a function of velocity approach to a straight line.

About 20 s before the maximum at EW 6 the amplitudes and shapes of the 0–18 km s^{-1} red distributions are similar to each other (left panel of Fig. 6). Also, about 40 s after the EE maximum the 9 km s^{-1} red distribution and the central one, at the location of the maximum, were similar to each other.

6.2. EEII, maximum at 13:42:00 UT

The maximum of this EE took place at EW position 5 around NS 20″ at 13:42:00 UT. The amplitude of the central velocity distributions clearly shows the increase and decrease (second panel, from left to right, of Fig. 3). The radiance at locations around the maximum is higher at red than at blue distributions. About 40 s before the

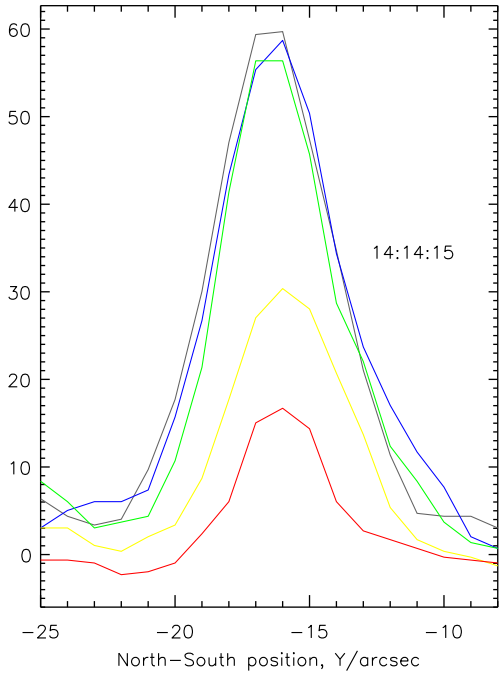

Fig. 6. NS red distributions observed 20 s before the maximum of EEI at $\sim 0.8''$ on its West side (left). In this case, the amplitude and shape for the 9–18 km s^{-1} and central distributions are similar to each other. At the time and location of the maximum (right) the 9 km s^{-1} red and central distributions are similar to each other. At the same location of the EE maximum, 40 s after it, the 9 km s^{-1} and central distributions are similar during approximately 40 s.

maximum, the red distributions are offset to the South respect the maximum of blue distributions.

After the maximum, at its location and at $\sim 0.8''$ on its West, an offset between the maximum of the 18 km s^{-1} blue and red distributions is seen. Also the 9 and 18 km s^{-1} blue and central distributions at $\sim 1.5''$ on the East of the maximum, observed $\sim$4.7 min after it, are similar to each other (as those of Fig. 6). The similar blue distributions are seen only in this EE at this time and location.

6.3. EEIII, maximum at 13:48:06 UT

This EE took place at EW position 5 around NS 17″ at 13:48:06 UT. The amplitude increases and decreases in the course of the observations (middle panel of Fig. 3). In this case, contrary to the other EE of the sample, the amplitude of the blue distributions is higher than the amplitude of the red distributions. No offsets are seen at the EE maximum and at close locations.

At $\sim 0.8''$ on the East side of the EE maximum, about 3 min before it, the blue distributions are either asymmetric or have two bumps (left panel of Fig. 7). At the blue 18 and 27 km s^{-1} distributions the southern bump is more intense. The 9 km s^{-1} blue distribution is asymmetric with the maximum at the South, which could indicate that two sources are present. The maximum of the 9 km s^{-1} distribution is even higher than the maximum at the central distribution. Also, it is worth to note that the maximum of the central bin distribution lies between the two bumps.

The red distributions at $\sim 0.8''$ on the East of the EE maximum also show two bumps $\sim$3 min before it (right panel of Fig. 7) but in this case the stronger source is the Northern one. The two bumps are located at the edges of the central distribution. In both cases the maxima are separated about 5″($\sim$4 Mm).

The red distributions at $\sim 1.5''$ at the East of the EE maximum showed two maxima, about 46 s before the EE maximum the Southern was the stronger (Fig. 8). After this, the Southern peak decreased and the Northern increased becoming the more intense $\sim$4 min after the EE maximum.

6.4. EEIV, maximum at 14:07:42 UT

This EE took place at EW 3 around NS −15″ at 14:07:42 UT (fourth panel, from left to right, of Fig. 3). The radiance at the maximum and around it is higher at red than at blue distributions. At $\sim 0.8''$ on the West of the EE maximum, about 1 min before it, the blue and red distributions are offset.

At $\sim 0.8''$ on the East of the maximum, about 1 min before it, the red 9–18 km s^{-1} and central distributions have similar shapes and amplitudes (as those of Fig. 6). The values are very similar to each other for a range of about 10″.

6.5. EEV, maximum at 13:55:35 UT

This EE took place at EW 5 around NS −13″ (right panel of Fig. 3). The radiance at locations around the maximum is higher at red than at blue distributions but 20 s before it, at $\sim 0.8''$ on the West, the radiance is higher at blue than at red.

Offsets between the maxima of blue and red distributions are seen in this EE at various locations. For example, at the time of the maximum of the 18, 27 and 36 km s^{-1} red distributions are at the South respect the maximum of the blue distributions. Also, 1 min before the EE maximum at the same location, the maxima of blue and red 27 km s^{-1} distributions are offset about 5″ (4 Mm).

At the time of the EE maximum the red maxima are also offset respect each other, the offset increasing with velocity (Fig. 9). Two minutes after the maximum at the central and 9–27 km s^{-1} blue distributions two maxima separated about 5″ are seen. The red distributions are asymmetric. The 36 km s^{-1} red distribution shows two peaks, separated about 13″. It is worth to note that the peak at NS −6″ is more intense at the 9–27 km s^{-1} distributions than at the central one. This situation is observed only in this case. At the first times observed there was no emission at $\sim$ NS −6. The emission at this location could either appear after the EE maximum or to be a source that during the EE maximum was located near NS −13″ but was not distinguishable, probably because was weak enough, and then drifted to the new

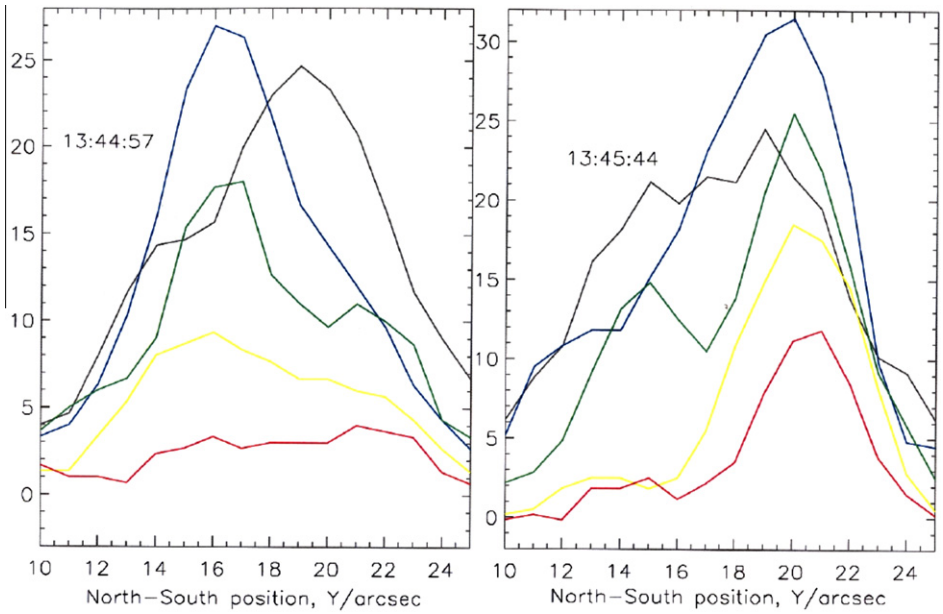

Fig. 7. NS blue distributions observed 3 min 8 s before the maximum of EEIII, ~ 0.8″ at its East (left). NS red distributions observed ~0.8″ at the West of the maximum, 2 min 21 s before it (right). At the 18 and 36 km s^{-1} blue and red distributions two bumps are separated by ~5″ (~4 Mm). The maximum of the central distribution lies between the blue bumps. The red bumps lie at the edges of the central one. The radiance of the 9 km s^{-1} blue distribution is higher than the central one at NS ~16 and that of the 9 km s^{-1} red distribution at NS ~20 is higher than the central one.

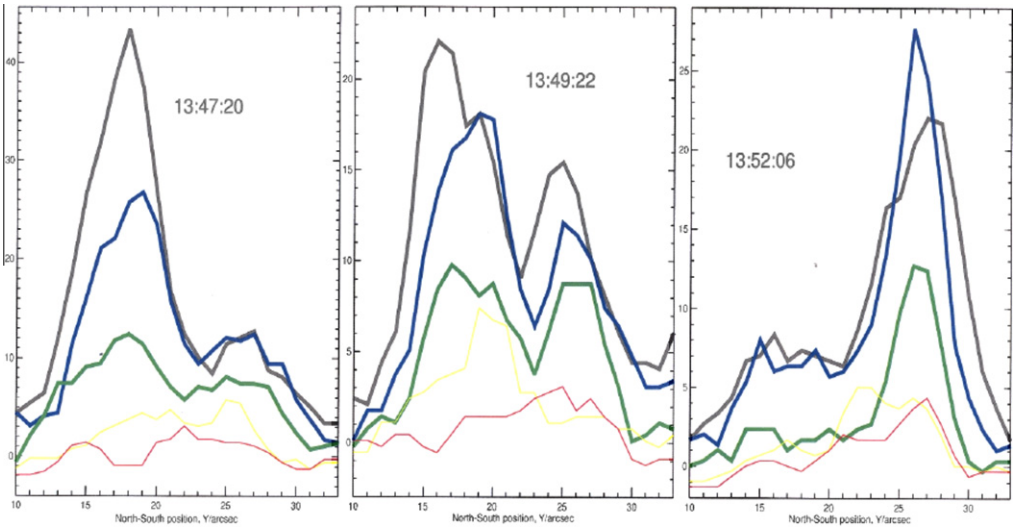

Fig. 8. Red distributions ~1.5″ at East of the EEII maximum, observed 46 s before it (left), 1 min 16 s after the maximum (middle) and 4 min after it (right). A peak at NS ~18 was more intense before the EE maximum, after it the peak decreased while a peak at NS ~26 increased. The peak at the 9 km s^{-1} red distribution is more intense than the central one.

location. If this would be the case then, the source would undergo a displacement of about 7 Mm in 2 min. In that case, the velocity of this source would be of ~60 km s^{-1}.

6.6. Offsets of the maxima of the sources at different velocities

At some locations it is observed that the maxima of different velocity sources of an EE are spatially offset respect each other. For example, the red sources at the time and location of the EEI maximum (left panel of Fig. 4), the offset increasing as the difference between velocities increases. The blue distributions at the same time and location are not offset respect each other. A similar situation is observed at the blue distributions of some EE sources.

For our case, the spectral features are similar to that of an inclined cylinder of Rompolt (1975) which, in the case of a only wavelength, gives a inclined line (respect the

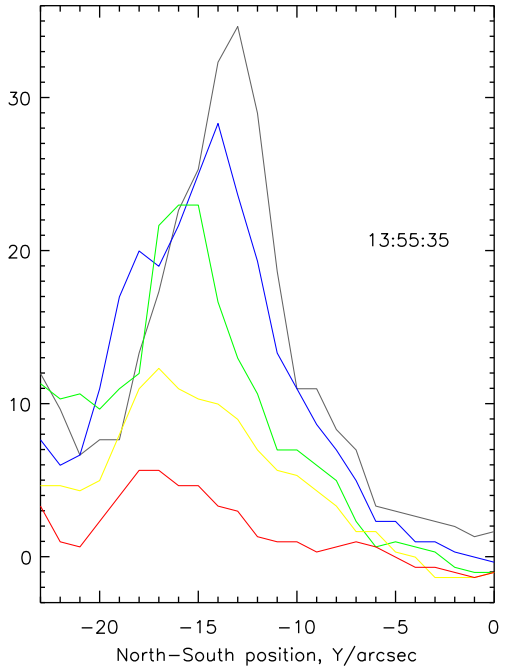

Fig. 9. The red distributions at the time and location of the EEV maximum. The maximum at the 36 km s^{-1} distribution (red curve) is about 5″ (4 Mm) to the South respect the maximum at the rest velocity (black line). The other maxima are less offset respect the central one.

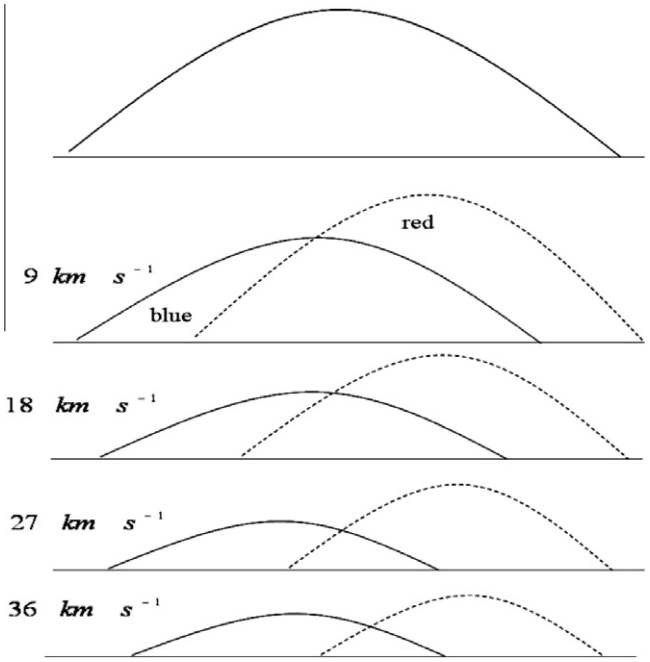

Fig. 10. Representation of the distributions observed at various times and locations as observed at EEI (Fig. 5).

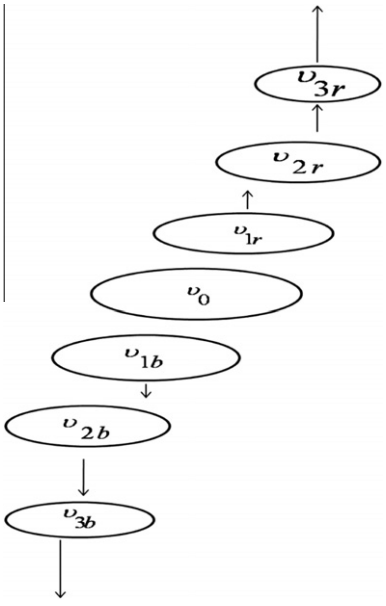

Fig. 11. The Doppler velocities of the sources respect their location projected onto the disk as observed at EEI (Fig. 5) where the sources of different velocities are offset as schematically shown in Fig. 10. The observer would be at the top of the figure and the solar surface at the bottom.

dispersion direction). Also, the case of a spherule leads to a tilted ellipse whose section in the slit direction is due to the emission by different elements of the spherule, each at one fixed wavelength.

The offset of the maximum of the higher velocity distributions in some cases is at the North and in other at the South respect the low velocity distributions. For example, at the maximum of EEV (Fig. 9) the 36 km s^{-1} red distribution maximum is at the South respect the lower velocity maxima. A 5″ (~4 Mm) offset between central and the 36 km s^{-1} red distributions maxima was observed.

This situation is reversed to that observed for the maxima of the red velocity distributions at 14:14:35 UT (left panel of Fig. 4) where the maximum of the 36 km s^{-1} source was at the North respect the maxima of the lower velocity distributions. However, in both cases the positions of the maxima and the velocities may be fitted with a linear relation which is further analyzed.

6.7. Offsets between blue and red sources

In some cases the offsets of the maxima are observed only on one Doppler sign distributions. For the same time and location the maxima of the other Doppler sign distributions are not offset respect each other. However, at other locations offsets at both, blue and red, distributions are observed. For example, for the distributions of Fig. 5. Solid lines are for blue and dashed for red distributions. Offsets between blue and red distributions are also seen at other times and positions, although the maximum of blue sources may be at the North and those of red at the South.

In Fig. 10 a cartoon of the conditions observed during more than 1 min at the East of the maximum of EEI (Fig. 5) is shown. In Fig. 11 a representation of the locations of the sources and their velocities (represented by

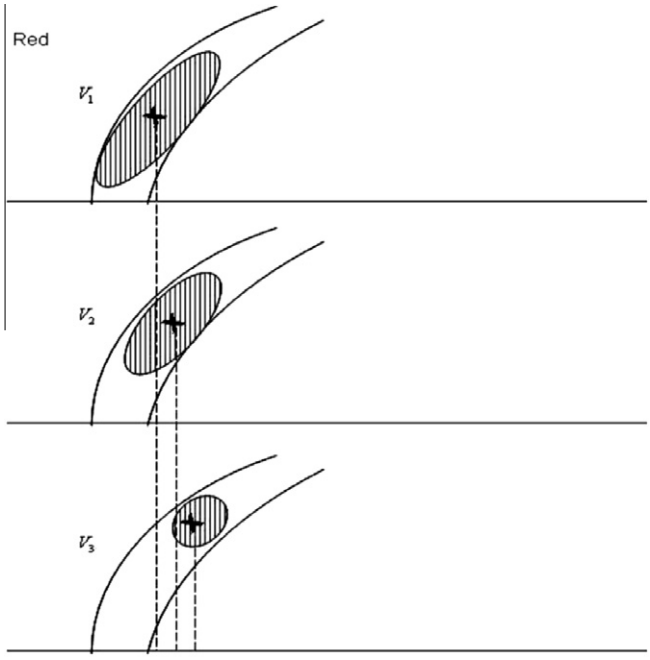

Fig. 12. Possible locations of different red shifted plasmas inside an arc. The observer looks to the apex of the arc from above. It means the LOS is on the top of the arc, in the direction parallel to the vertical lines. The crosses at the center of the sources indicate the possible location of the maximum radiance at the given velocity source. The rest Doppler velocity source is the more extended. The location of the maximum radiance of the red sources is spatially offset to lower locations of the arc. The largest velocity red source v_3 is the less extended and its maximum is the most separated from the center of the rest wavelength source.

arrows) is given. In Fig. 12 a possible scenario for the sources in magnetic arcs is shown.

The size along the slit direction of the spectral emission is largest at the rest wavelength and decreases as the velocity grows. This seems similar to Rompolt (1975) spectral features of a spherule. However, it is worth to point out that his computations were done taking into account only one wavelength at each spatial pixel of the slit. The extended sources of Figs. 10 and 11 represent the distributions along the slit, that we found, at each spectral pixel.

6.8. Similar amplitudes between different velocity distributions

In some cases, the amplitudes of the distributions of different bins are similar to each other. For example, as may be seen from Fig. 5 the central distribution is very similar in shape and amplitude to the 9 km s^{-1} and 18 km s^{-1} distributions over the whole source. This means that, the radiance is almost the same in a velocity range of 18 km s^{-1}. Sources with different velocities but similar shapes and amplitudes are also observed at other locations and times. This indicates that the distributions of the given velocity range are similar not just by chance but because they reflect the physical conditions at some locations of the EE sources themselves.

6.9. Asymmetric shapes of the sources

Simple shapes with only one peak are seen at many locations of the EE, including the maximum. However, at some given times and locations the distributions are either asymmetric or they show two bumps.

In general, the time variations of the 36 km s^{-1} distributions do not coincide with variations at the smaller velocity sources. They can take completely different shapes in less than a minute. This behavior is seen at both, blue and red high velocity distributions but more frequently at the red ones. For example, the red 36 km s^{-1} distribution at Fig. 9 showed a maximum at NS $\sim -17''$ that moved to NS $\sim -14''$ in less than 1 min (central panel). Between these two times the maximum of the 36 km s^{-1} blue channel distribution moved from NS $-19''$ to NS $-16''$.

The blue distributions of the left panel of Fig. 7 correspond to a location at the East of the EE III maximum while the red distributions to the West (right panel). Both, blue and red distributions are asymmetric but the maxima of blue distribution takes place at NS $\sim$16 while the maxima of the red at NS $\sim$20. The maximum of the central distribution took place between the two bumps. The same situation was observed about 1.5 min after the maximum of EEII where also asymmetric shapes or two bumps were observed at the blue distributions whose maxima were located at the edges of the wide central distribution observed at this time. In these cases, one of them is very intense, even more intense than the central one. The bumps could be due to the presence of two sources. On the other hand, the red distributions of Fig. 8 show a case where the maximum of the central distributions does not lie between the two bumps at red or blue distributions.

7. Discussion

The distributions analyzed here were obtained from the amplitudes of different velocity bins of the spectral line at a series of NS positions around the location of the maximum radiance of each EE.

As seen from the above results, these distributions allow to identify common characteristics of the EE sources.

1. (a) Offsets between the maxima of either red or blue different velocity distributions that could be seen from the location of the maximum itself to 1.5″ from it. (b) Offsets between maxima of blue and red distributions seen at 0.8″ from the maximum of the EE. 2. At some other locations, at 0.8″ from the maximum, different velocity distributions are similar to each other in shape and amplitude. 3. Also, at other locations the shapes show two bumps or are asymmetric.

These characteristics are commonly observed at the EEs but not always at the same time in a given EE. In a given EE the three characteristics could be seen while at other EE one or two of them could be absent. This could be due to the narrow field of view of the observations (6 slit

EW positions) and then for a given case one or two features could be out of that field.

As mentioned above, dividing the non-Gaussian spectral profile into various Gaussian functions has been a method used to estimate the parameters of flows at EEs. Here, based on the different velocities, we identified a correlation between the maximum radiance at the spatial distributions and the Doppler flow. Also, the similarity of the 0–18 km s^{-1} radiance distributions could be identified only based on the method of analyzing the NS distributions at different velocity channels of an emission line. The size of the events studied here is close to the instrument spatial resolution, i.e. 2″. Even at such small scales a diversity of distributions can be observed.

7.1. The relation between locations and velocities of the sources

This section has to be brought to the point. Using the positions of the maxima with offsets and the corresponding velocities we find linear relations between velocity and position. The observed $\frac{v_r}{r}$ ratio seems to correspond to the geometry of a circumference which could represent a loop where the source could be constrained. The slope ($\frac{v_r}{r}$ ratio) results of $\sim 20-30$ km s^{-1} Mm^{-1}.

For a source moving inside an arc with constant velocity (v_0) the observed velocity depends on the angle between the arc and the observer (see the cartoon of Fig. 12). If the observer sees to the apex of a circumference then the observed velocity (v_r) in terms of the radius of the circumference (r_0) is

$$v_r = v_0 \frac{r}{r_0} \tag{1}$$

where $r = r_0 cos\theta$ and θ is the angle between the horizontal (in this case assumed the solar surface) and the radio vector to the location of interest on the circumference (in this case the location of the maximum radiance at a given velocity distribution). The linear relation between the maxima of the distributions and their velocity agrees with the velocity of a source inside an arc. The offset of the maxima could result from magnetic reconnection where the produced flows are channeled inside the arcs (Moore et al. (1999)) similarly to small cool jets at the TR (Kamio et al., 2009), but in this case the reconnection could take place between two different sized arcs or in interacting loops, where one of them is smaller, as observed in coronal loops (Hanaoka, 1996). The similarity of the radiance distributions (Fig. 6) could be due to the emission in the smaller loop, as in the cartoon by Mendoza-Torres and Niembro-Hernández (in press).

The distributions with two bumps or asymmetric shape could also be the result of emission from magnetic arcs. In flares the radio as well as the soft X-ray emission comes from different legs of the magnetic arcs (Aschwanden and Benz, 1997; Hanaoka, 1996). A similar situation could take place at EE. The distance between the maxima of the distributions is 5–7 Mm. Assuming that they correspond to sources at the arc bases the radius would be $r_0 = 2.5$–3.5 Mm. Using the smallest and the largest values for radius and gradient, the velocity inside the arc would be $v_0 = 50$–105 km s^{-1}. The largest of the above velocities is near to that of those typically seen at EE.

As seen above, sometimes the higher velocity sources are on the South respect the lower ones and in other cases the opposite situation is observed. This could be interpreted as a result of reconnection either on one side of the magnetic tube or at the other one.

7.2. Extensions of different velocity sources

At some locations different velocity sources (18, 9 km s^{-1} and central one) have the same extension, at least projected onto the solar disk (Fig. 6). This is more frequently observed at the red distributions. The similar extensions could result if the flow is slowed down from a given velocity to the rest one in a very short distance.

At some locations the amplitude of the low velocity red distributions is even higher than the central one indicating a large release of radiative energy (this also happens for blue distributions but less frequently). A deceleration in a short spatial scale from the 18 km s^{-1} source to the central one could transform kinetic energy into radiation, leading to enhanced blue and red emission. A flow directed towards the solar surface could be stopped at short distances since it finds high density regions. The similar curves could be due to a flow that goes to a leg of the smaller magnetic tube (in the case of interacting loops) and therefore its location does not coincide with those of the offsets.

8. Conclusions

The analysis of the spatial distributions of sources of EE observed at different velocity bins of the spectral line allows distinguishing some characteristic features of the nature of EE.

At some locations there is an offset between maxima of the different velocities, either of blue or red distributions.

At some other locations the blue and red sources are offset, the offset decreasing with velocity.

Similar shapes and amplitudes of the 18, 9 km s^{-1} and central distributions are seen at some locations at red in various EE but only in one case in blue sources.

In other cases two bumps are observed the central distribution maximum lies between the two bumps. These characteristics agree with an scenario where magnetic reconnection takes place inside magnetic arcs.

References

Aschwanden, M.J., Benz, A.O. ApJ 480, 825, 1997.
Brueckner, G.E., Bartoe, J.-D.F. ApJ 272, 329, 1983.
Dere, K.P. Adv. Space Res. 14, 13, 1994.
Hanaoka, Y. Sol. Phys. 165, 275, 1996.

Innes, D.E., Inhester, B., Axford, W.I., Wilhelm, K. Nature 386, 811, 1997.
Kamio, S., Hara, H., Watanabe, T., Curdt, W. AA 502, 345, 2009.
Mendoza-Torres, J.E., Niembro-Hernández, R.T., Astronomical Society of the Pacific Conference Series, vol. 463, in press.
Mendoza-Torres, J.E., Wilhelm, K., Lara, A. AA 495, 613, 2009.
Moore, R.L., Falconer, D.A., Porter, J.G., Suess, S.T. ApJ 526, 505, 1999.
Ning, Z., Innes, D.E., Solanki, S.K. AA 419, 1141, 2004.
Pérez, M.E., Doyle, J.G., Erdélyi, R., Sarro, L.M. AA 342, 279, 1999.
Rompolt, B. Sol. Phys. 41, 329, 1975.
Teriaca, L., Madjarska, M.S., Doyle, J.G. AA 392, 309, 2002.